Dynamic Modeling and Stability Analysis of Articulated Frame Steer Vehicles

Yuping He*, Amir Khajepour*, John McPhee†, and Xiaohui Wang*
*Mechanical Engineering and †Systems Design Engineering
University of Waterloo, Ontario, Canada, N2L 3G1

Abstract

The stability analysis of articulated frame steer vehicle models is presented. To reveal the relationship between the "oversteer" and "jack-knife" motion modes based on a 2 degree of freedom (DOF) and 3 DOF vehicle models, respectively, the results derived from these models are investigated and compared. To identify the effects of design variables on the lateral stability of the vehicle, a more realistic model with a hydraulic rotary valve and dynamic tire models is generated on the basis of the 3 DOF model and the results derived from these models are examined and compared. Similar to traditional articulated vehicles, the jack-knife and "snaking" modes were identified from practical operations of the articulated frame steer vehicles. Results demonstrate that, with the decrease of the angular spring (representing the hydraulic cylinder between the front and rear sections of the vehicle) stiffness coefficient, the oversteer mode evolves into the jack-knife mode. Compared with the static tire model, the effects of dynamic transient lateral tire force degrades the stability of the vehicle over the lower speed range. Results also illustrate that, with the fluid leakage either in the rotary valve or in the hydraulic cylinder, the stability of the oversteer mode dominated motion degrades. On the contrary, in the case of snaking mode dominated motion, the introduction of the fluid leakage will improve the stability of the vehicles.

Key Words: stability analysis, articulated frame steer vehicles, combined mechanical and hydraulic system, rotary valve, modeling and simulation

Nomenclature

The subscript i goes from 1 to 4 to represent the four wheels. The subscript j runs from 1 to 2 to denote the front and rear sections of the vehicle. C_1 and C_2 are the centers of mass of front and rear sections of the vehicle. Other symbols are explained in Table 1.

Table 1: Definitions of symbols

a	distance from C_1 to front axle;	Q_L	fluid leakage across cylinder;
a_{yj}	lateral acceleration at C_j;	Q_r	flow rate through right chamber of cylinder;
$\mathbf{A}$	system matrix in governing equations;	$\overline{Q}_r$	normalized value of Q_r;
A_i	metering orifice areas, $i = 1, 2, 3, 4$;	Q_{max}	maximum flow rate;
A_p	area of hydraulic cylinder;	r	radius of inner cylinder of rotary valve sleeve;
b	distance from C_1 to pin joint;	$\mathbf{r}$	state variable vector;
$\mathbf{B}$	system matrix in governing equations;	R	rolling radius of tire;
B	bulk modulus of hydraulic fluid;	R_x, R_y	pin joint reaction forces;
$\mathbf{C}$	system matrix in governing equations;	t	time;
C_d	flow coefficient for metering orifices;	t_a	half of front and rear axle length;
C_{tj}	aligning torque coefficient of front or rear tire;	T_{aj}	aligning torque summed over axle j;
C_{xj}	longitudinal force coefficient of front or rear tire;	T_j	steering torque on section j;
C_{yj}	lateral force coefficient of front or rear tire;	T_N	control torque about pin joint;

C_{Yj}	cornering stiffness coefficient of front or rear tire;
C_ϕ	torsional damping coefficient;
d	constant moment arm;
e	distance from pin joint to C_2;
f	distance from C_2 to rear axle;
F	hydraulic actuator force;
I_j	yaw inertia of section j about C_j;
I_w	wheel spin inertia;
k_0	valve orifice area constant;
k_c	a constant;
K	understeer gradient;
K_{L0}	cylinder leakage constant;
K_i	constants, $i = 1, 2, 3$;
K_ϕ	torsional spring stiffness coefficient;
l_0	valve zero displacement leakage coefficient;
l_a	a constant;
L	half of the hydraulic cylinder length;
L_j	length of section j of vehicle;
m_j	mass of section j of vehicle;
m	hydraulic piston displacement;
L	length of hydraulic cylinder;
L_j	length of section j of vehicle;
m_j	mass of section j of vehicle;
m	hydraulic piston displacement;
n	valve linear displacement;
P_0	tank pressure;
P_l	left cylinder chamber pressure;
P_r	right cylinder chamber pressure;
P_s	pump pressure;
$\overline{q}$	perturbation of $\overline{Q}$;
Q	flow rate through the hydraulic cylinder;
$\overline{Q}$	normalized value of Q;
Q_i	flow rates, $i = 1, 2, 3, 4$;
Q_l	flow rate through left chamber of cylinder;
$\overline{Q}_l$	normalized value of Q_l;
T_{wi}	aligning torque on tire i;
u	forward speed of vehicle;
u_j	forward speed of section j;
v	lateral speed of vehicle;
v_j	lateral speed of section j;
$\overline{v}_m$	perturbation of $\overline{V}_m$;
V	velocity of front section;
V_j	velocity at axle j;
V_m	fluid volume through the hydraulic cylinder;
$\overline{V}_m$	normalized value of V_m;
V_{m0}	half total fluid volume;
X_j	longitudinal tire force summed over axle j;
X_{wi}	longitudinal tire force on tire i;
Y_j	lateral tire force summed over axle j;
Y_{wi}	lateral tire force on tire i;
Z_j	front or rear static tire load;
α_j	slip angle of front or rear tire;
α_2	equivalent slip angle of rear tire;
β	angular displacement between spool and sleeve;
$\overline{\beta}$	normalized value of β;
β_1	angular displacement at upper end of torsion bar;
β_2	angular displacement at lower end of torsion bar;
ϕ	articulated angle;
$\overline{\phi}$	normalized value of ϕ;
ϕ_c	desired articulated angle;
$\overline{\phi}_c$	normalized value of ϕ_c;
ϕ_0	initial value of articulated angle;
ϕ_{max}	maximum articulated angle;
ρ	fluid density;
θ_i	spin angle of tire i;
γ	yaw velocity of vehicle;
γ_j	yaw velocity of section j;
σ_t	relaxation length for tire torsional motion;
σ_x	relaxation length for tire longitudinal motion;
σ_y	relaxation length for tire lateral motion.

1 Introduction

For off-road vehicles, requirements of mobility, maneuverability, and traction often result in the articulated frame steer configuration [1, 2, 3]. These vehicles are used in forestry, construction, etc. "Although designed primarily around their off-road operation, they often travel substantial distances on road, so their steering and handling behaviour both on and off the road is important" [2].

For traditional articulated vehicles with Ackerman steering mechanisms, e.g truck-trailer combinations, three typical instability modes, as shown in Figure 1, have been identified [4, 5, 6]: (1) Snaking: trailer yaw oscillation; (2) Jack-knife: truck yaw motion (nonperiodic instability); (3) Trailer swing: trailer yaw motion (nonperiodic instability). Note that the jack-knife and trailer swing motion modes are generally associated with braking and steering operation conditions. For articulated frame steer vehicles, it has been qualitatively reported by manufacturers and drivers that these vehicles are prone to "jack-knife" about the articulated point at any speed and exhibit "snaking".

Since the unstable modes represent potentially hazardous situations, researchers should analyse

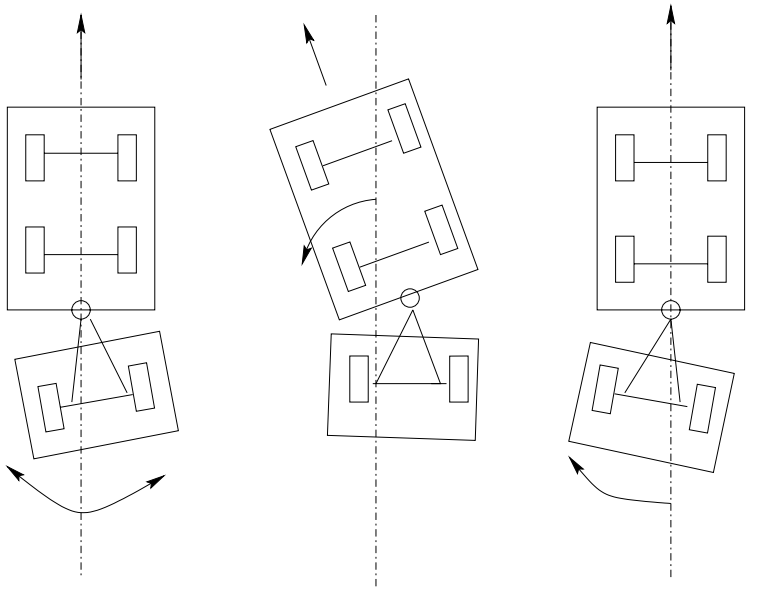

Figure 1: Unstable motion modes of traditional articulated vehicles

dynamic vehicle systems, determine where the various stability boundaries lie, and offer design instructions for improving vehicle stability. The existing investigations may be classified into two groups. In the first group of studies reported by Jindra [9] and others, the vehicle is assumed to negotiate a steady turn at constant velocity and the governing equations are linearized. The stability of the resulting equations is then investigated by the Routh's criterion or by examining the eigenvalues of the characteristic equation. In the other approach used by Vlk [10] and others, the nonlinear differential equations are integrated numerically to obtain the response to some arbitrary inputs.

"It is well-known that a mechanical system which is subject to non-conservative forces may become dynamically unstable under certain conditions" [7]. In the stability analysis, the Hurwitz criterion indicated that self-excited vibrations resulting from the non-conservative forces were developed beyond a critical forward speed, thus giving roots to the concept of critical speed [4]. In an articulated frame steer vehicle, the non-conservative forces may arise at the contact point between the tires and road due to lateral forces, aligning torques, and longitudinal forces.

In a rail vehicle, the non-conservative forces arise at the contact point between the wheels and rails; the rail vehicle may also exhibit an unstable behavior called "hunting". The physical basis of wheel/rail and tire/road (for conventional road vehicles) rolling contact mechanics are to a great extent the same [8]. This similarity is reflected in the existence of asymmetric matrices in the governing equations for both rail and road vehicles. Corresponding to the hunting phenomenon for rail vehicle wheelsets, there exists the shimmy phenomenon for road vehicle steering systems. Moreover, similar asymmetric matrices are found in rotor dynamics, wind turbine dynamics, and aeronautics.

For articulated frame steer vehicles, since the front and rear sections affect one another due to inner forces acting at their articulated pivot point, the handling characteristics of these vehicles are much more complex than the behavior of single frame vehicles [4]. Little attention has been paid to the stability analysis of these vehicles. In the 1980s, however, two relevant papers were published. In

1983, Crolla and Horton [2] reported their stability analysis results based on a 3 degrees of freedom (DOF) planar vehicle model. In their model, an angular spring was introduced to represent the hydraulic cylinders (used to manipulate the articulated angle for the purpose of steering) between the front and rear sections of the vehicle. They highlighted stability problems resulting in a lateral oscillating motion of the vehicle. Their results were consistent with results reported by various manufacturers qualitatively. In 1986, the same authors [3] reported their results based on a combined mechanical and hydraulic vehicle model. The model was generated on the basis of their previous 3 DOF model, with the introduction of a sliding valve and hydraulic steering ram model. It was shown that both oscillatory and nonperiodic instabilities may occur with this type of vehicle. It was further demonstrated that the most sensitive design feature is the hydraulic steering system, which governs the effective torsional stiffness around the articulated pivot point.

In this work, to disclose the relationship between the "oversteer" and "jack-knife" motion modes based on 2 DOF and 3 DOF articulated frame steer vehicle models, respectively, the results derived from these models are investigated and compared. To further identify the effects of design variables on the lateral stability of the vehicle, a hybrid model with typical hydraulic rotary valve and dynamic tire models is generated on the basis of the 3 DOF model and the results derived from these models are examined and compared. The unstable motion modes derived from the hybrid model is originally interpreted by those based on the 2 DOF model. By means of a parameter study, the conflicting character of the fluid leakage either in rotary valve or in hydraulic cylinders is revealed: in the "oversteer" mode dominated motion, the introduction of the fluid leakage has negative effect on the stability of the vehicle; in the "understeer" mode dominated motion, however, it has a positive effect. In the following sections, the vehicle models are described; then numerical results for stability analysis based on the models are compared and investigated; finally a parameter study for the stability of the vehicles based on the hybrid model is carried out.

2 Vehicle System Modeling

In this section, the 2 DOF, 3 DOF, and hybrid vehicle model are described.

2.1 2 DOF Rigid Body Vehicle Model

The 2 DOF "bicycle" model is shown in Figure 2. The model consists of front and rear sections connected by a pin joint at point P and a hydraulic cylinder. The front and rear wheels are replaced by single wheels at the center of front and rear axles. Instead of using the wheels for steering, the vehicle uses its frame with articulated angle ϕ. The $x - y$ coordinate system is fixed to the front section at C_1. The x axis aligns with the body centered axis of the front section and the y axis is directed to the right viewed along the x axis.

To derive the linear governing equations of motion of the vehicle model, it is assumed that: forward speed u is constant; lateral tire forces, Y_1 and Y_2, are the only external forces; articulated angle ϕ is small, so that $cos(\phi) = 1$, $sin(\phi) = 0$; once ϕ is generated, the front and rear sections of the vehicle are rigidly connected; only lateral motion and yaw motion are considered; products of v, γ, and ϕ are small enough to ignore. With these assumptions, the instantaneous velocities (see Figure 2) at front tire, point C_1, and rear tire are V_1, V, and V_2, respectively. The instantaneous center of zero velocity is point O. For the vehicle model, the nominal values for geometric, inertial, and tire

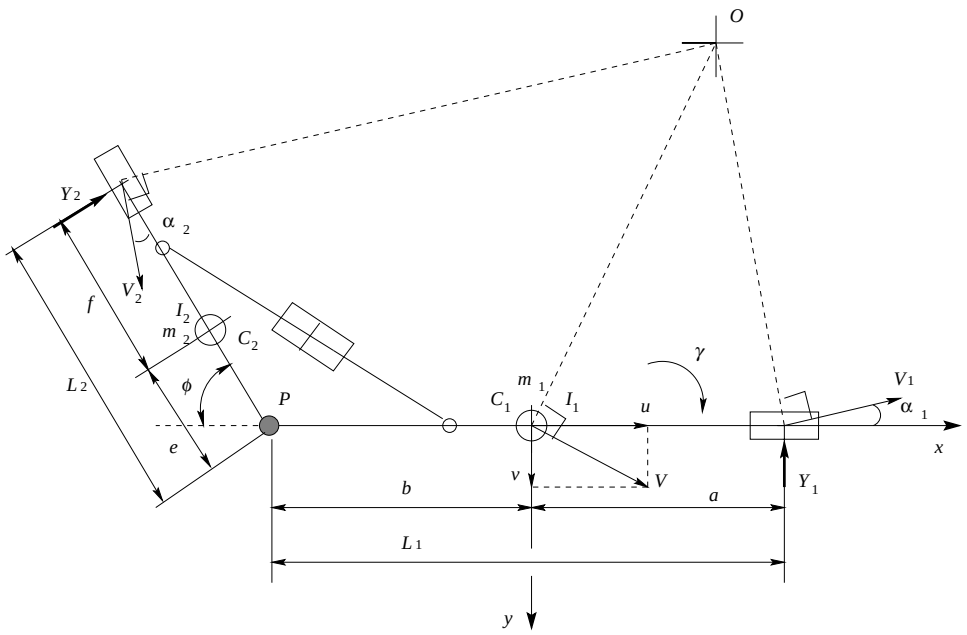

Figure 2: 2 DOF vehicle model

property parameters, mainly taken from one of Timberjack grapple skidders as shown in Figure 3, are listed in Table 2.

Table 2: Nominal design variables

$m_1 = 7010\ [kg]$	$L_2 = 1.953\ [m]$	$t_a = 1.13\ [m]$	$Q_{max} = 2.1 \cdot 10^{-3} [m^3/s]$
$I_1 = 7010\ [kg \cdot m^2]$;	$K_\phi = 2 \cdot 10^8\ [Nm/rad]$	$R = 1.20\ [m]$	$P_s = 2.07 \cdot 10^7\ [N/m^2]$
$m_2 = 8590\ [kg]$;	$C_\phi = 0.0\ [Nms/rad]$	$A_p = 5.03 \cdot 10^{-3}\ [m^2]$	$B = 1.72 \cdot 10^9\ [N/m^2]$
$I_2 = 8590\ [kg \cdot m^2]$;	$C_{y1} = 6.0\ [1/rad]$	$d = 0.7\ [m]$	$\phi_{max} = 15\ [deg]$
$a = 0.8635\ [m]$;	$C_{y2} = 6.0\ [1/rad]$	$\sigma_y = 1.0$	$l_0 = 0.0$
$b = 0.8635\ [m]$;	$C_{t1} = 0.4\ [m/rad]$	$\sigma_x = 1.0$	$k_0 = 0.707$
$e = 0.9765\ [m]$;	$C_{t2} = 0.4\ [m/rad]$	$\sigma_t = 1.0$	$K_{L0} = 0.01$
$f = 0.9765\ [m]$;	$C_{x1} = 6.5$	$I_w = 287.0\ [kg \cdot m^2]$	
$L_1 = 1.727\ [m]$;	$C_{x2} = 6.5$	$V_{m0} = 1.8 \cdot 10^{-3}\ [m^3]$	

With the above assumptions, based on d'Alembert's principle, we have:

$$\begin{cases} Y_1 + Y_2 = m_1 a_{y1} + m_2 a_{y2} \\ Y_1 a - Y_2(b + L_2) = [I_1 + I_2 + m_2(b^2 + e^2 - 2be)]\dot{\gamma} - m_2 a_{y2}(b + e) \end{cases} \tag{1}$$

where

$$\begin{cases} a_{y1} = \dot{v} + u\gamma \\ a_{y2} = \dot{v} + u\gamma - (b + e)\dot{\gamma} \end{cases} \tag{2}$$

Figure 3: Timberjack grapple skidder

and

$$\begin{cases} Y_1 = C_{Y1}\alpha_1 \\ Y_2 = C_{Y2}\alpha_2^{'} \\ \alpha_1 = (v + a\gamma)/u \\ \alpha_2^{'} = \alpha_2 + \phi \\ \alpha_2 = [v - (b + L_2)\gamma]/u \\ C_{Y1} = C_{y1}Z_1 \\ C_{Y2} = C_{y2}Z_2 \end{cases} \tag{3}$$

Based on equations (1), (2), and (3), the governing equations of motion in matrix form become:

$$\mathbf{A}\dot{\mathbf{r}} = \mathbf{B}\mathbf{r} + \mathbf{C}\phi \tag{4}$$

where $\mathbf{r} = [v \ \ \gamma]^T$ and the matrices $\mathbf{A}$, $\mathbf{B}$, and $\mathbf{C}$ are offered in the Appendix. In the case $\dot{v} = 0$ and $\dot{\gamma} = 0$, based on equation (4), the steady state solution can be obtained. The ratio of yaw velocity to the articulated angle (γ/ϕ, called "yaw velocity gain") is given by:

$$\frac{\gamma}{\phi} = \frac{u/(L_1 + L_2)}{1 + Ku^2} \tag{5}$$

where

$$K = [(1/C_{Y1} + 1/C_{Y2})(b + e)m_2 + (m_1 + m_2)(a/C_{Y2} - (b + L_2)/C_{Y1})]/(L_1 + L_2)^2 \tag{6}$$

As for the case of conventional vehicles [17], the "understeer gradient" K can be used to determine understeer ($K > 0$), oversteer ($K < 0$), neutral steer ($K = 0$) features of articulated frame steer vehicles [2].

2.2 4 DOF Vehicle Model

To improve the 2 DOF model described previously, as shown in Figure 4 (a), in the first case, an angular spring with coefficient K_ϕ and an angular damper with coefficient C_ϕ are introduced to simulate the steering hydraulic cylinders of the vehicle. In the second case, instead of using the spring and damper, an actuator N is introduced to represent the hydraulic cylinders. For this planar model, as illustrated in Figure 4 (b), two sets of coordinate axes are used. The $x_1 - y_1$ is fixed to the front section at its center of mass where the x_1 axis aligns with the body centered axis and y_1 axis is directed to the right viewed along the x_1 axis. Similarly, the $x_2 - y_2$ is introduced and fixed to the rear section of the vehicle. The motions concerned are lateral, longitudinal, and yaw motions of the front section and yaw motion of the rear section, denoted as u_1, v_1, γ_1, and γ_2, respectively. The nominal values for geometric and inertial parameters of the veicle are listed in Table 2.

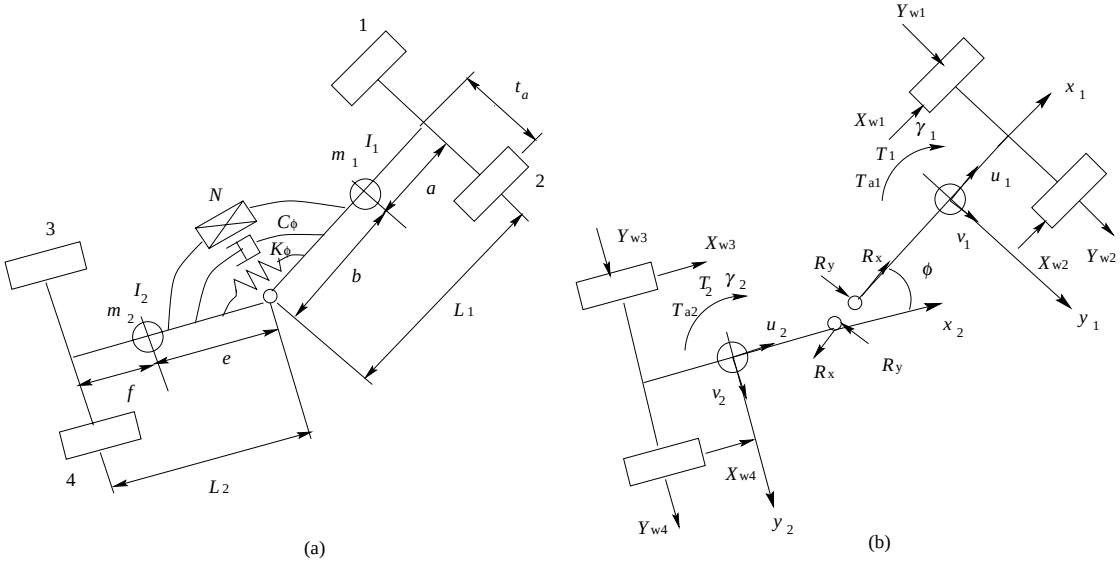

Figure 4: Vehicle configuration (a) and vehicle forces (b)

The forces acted on the vehicle's front and rear sections are pin joint reaction forces, steering torques on front and rear section, and tire forces. The tire forces include tire aligning torques summed over front and rear axles, longitudinal tire forces, and lateral tire forces.

Based on Newtonian methods, the equations of motion of the front section of the model are:

$$\begin{cases} m_1(\dot{u}_1 - v_1\gamma_1) = X_1 + R_x \\ m_1(\dot{v}_1 + u_1\gamma_1) = Y_1 + R_y \\ I_1\dot{\gamma}_1 = T_1 + T_{a1} + aY_1 + t \triangle X_1 - R_y b \end{cases} \tag{7}$$

where

$$\begin{cases} X_1 = X_{w1} + X_{w2} \\ Y_1 = Y_{w1} + Y_{w2} \\ \triangle X_1 = X_{w1} - X_{w2} \end{cases} \tag{8}$$

For the rear section, the equations of motion are:

$$\begin{cases} m_2(\dot{u}_2 - v_2\gamma_2) = X_2 - R_x c - R_y s \\ m_2(\dot{v}_2 + u_2\gamma_2) = Y_2 + R_x s - R_y c \\ I_2\dot{\gamma}_2 = T_2 + T_{a2} - fY_2 + t_a \triangle X_2 + R_x es - R_y ec \end{cases} \tag{9}$$

where

$$\begin{cases} X_2 = X_{w3} + X_{w4} \\ Y_2 = Y_{w3} + Y_{w4} \\ \triangle X_2 = X_{w3} - X_{w4} \\ c = cos(\phi) \\ s = sin(\phi) \end{cases} \tag{10}$$

The articulated angle between the front and rear sections is defined by

$$\phi = \phi_0 + \int_0^t (\gamma_2 - \gamma_1)dt \tag{11}$$

The two sections are connected at the pin joint and the velocities of the pin joint using either set of local coordinate systems must be compatible. Hence, we have

$$\begin{cases} u_2 = u_1 c + (v_1 - b\gamma_1)s \\ v_2 + e\gamma_2 = (v_1 - b\gamma_1)c - u_1 s \end{cases} \tag{12}$$

Thus, the accelerations are

$$\begin{cases} \dot{u}_2 = \dot{u}_1 c - u_1(\gamma_2 - \gamma_1)s + (\dot{v}_1 - b\dot{\gamma}_1)s + (v_1 - b\gamma_1)(\gamma_2 - \gamma_1)c \\ \dot{v}_2 = -\dot{u}_1 s - u_1(\gamma_2 - \gamma_1)c + (\dot{v}_1 - b\dot{\gamma}_1)c - (v_1 - b\gamma_1)(\gamma_2 - \gamma_1)s - e\dot{\gamma}_2 \end{cases} \tag{13}$$

Substituting for u_2, v_2, $\dot{u}_2$, and $\dot{v}_2$ in equation set (9) and eliminating reaction pin joint forces R_x and R_y from the resulting equation set and (7), the following equation set is derived.

$$\begin{cases} m_0\dot{u}_1 + m_2 e\dot{\gamma}_2 s = m_0 v_1\gamma_1 - m_2 b\gamma_1^2 - m_2 e\gamma_2^2 c + F_1 \\ m_0\dot{v}_1 - m_2 b\dot{\gamma}_1 - m_2 e\dot{\gamma}_2 c = -m_0 u_1\gamma_1 - m_2 e\gamma_2^2 s + F_2 \\ m_2 b(e\dot{\gamma}_2 c - \dot{v}_1) + (I_1 + m_2 b^2)\dot{\gamma}_1 = T_1 + T_{a1} + aY_1 + t_a \triangle X_1 - bX_2 s - bY_2 c + m_2 b(u_1\gamma_1 + e\gamma_2^2 s) \\ m_2 e(\dot{u}_1 s - \dot{v}_1 c + b\dot{\gamma}_1 c) + (I_2 + m_2 e^2)\dot{\gamma}_2 = T_2 + T_{a2} + t_a \triangle X_2 - L_2 Y_2 + m_2 e\gamma_1(u_1 c + v_1 s - b\gamma_1 s) \end{cases} \tag{14}$$

where

$$\begin{cases} m_0 = m_1 + m_2 \\ F_1 = X_1 + X_2 c - Y_2 s \\ F_2 = Y_1 + X_2 s + Y_2 c \end{cases} \tag{15}$$

In the absence of the actuator N, restraining torques are produced by the torsional spring and damper for the straight-running conditions $\phi = 0$. Thus, the internal torques T_1 and T_2 are given by

$$\begin{cases} T_1 = K_\phi\phi + C_\phi\dot{\phi} \\ T_2 = -K_\phi\phi - C_\phi\dot{\phi} \end{cases} \tag{16}$$

In the absence of the torsional spring and damper, the hydraulic actuator may generate a control torque T_N about the pin joint for steering the vehicle. Thus the internal torques T_1 and T_2 may be calculated by

$$\begin{cases} T_1 = -T_N \\ T_2 = T_N \end{cases} \tag{17}$$

With small disturbances and at constant forward speed, the following simplifications may be made: the forward motion equation is ignored, longitudinal tyre forces are absent, the aligning torques T_{a1}, T_{a2}, and the control torque T_N are not considered, and $cos(\phi) = 1$, $sin(\phi) = \phi$. All products of small variables are ignored. The lateral forces Y_1 and Y_2 are calculated according to equation set (3). Thus, the equation set (14) may be simplified and the 4 DOF model reduced to a 3 DOF model. The resulting equations of motion for the 3 DOF model may be cast in a matrix form as

$$\mathbf{A}\dot{\mathbf{r}} = \mathbf{B}\mathbf{r} \tag{18}$$

where $\mathbf{r} = [v_1 \;\; \gamma_1 \;\; \gamma_2 \;\; \phi]^T$ and the matrices $\mathbf{A}$ and $\mathbf{B}$ are listed in the Appendix.

2.3 Hybrid Mechanical and Hydraulic Vehicle Model

2.3.1 Configuration of the Hybrid Vehicle Model

In Figure 4 (a), if the torsional spring and damper are eliminated and hydraulic actuator N is expressed in detail as a hydraulic power steering system, we have the model as shown in Figure 5.

The hydraulic system consists of a rotary valve, a hydraulic cylinder and piston, and a constant fluid flow pump. The valve has three components, a spool, valve sleeve, and a torsion bar. Figure 6 illustrates the cross section of a rotary valve. Axial slots in the valve sleeve inside diameter and the spool outside diameter interact to create flow paths that guide fluid through the valve. The slots in the valve sleeve are larger than their mating lands in the spool; therefore in the on-center position as shown in Figure 6, the fluid is allowed to flow with minimal restriction through the valve and there is no differential pressure across the cylinder. When torque is acting at the steering wheel and transmitted to the valve spool by the upper column, the spool rotates directly with the steering wheel angle β_1. Note that at the upper end of the torsion bar, the spool is pinned with the torsion bar. At the lower end of the torsion bar, the valve sleeve, torsion bar, and pinion are pinned together. Excited by the torque at the steering wheel, the torsion bar twists with an angle $\beta = \beta_1 - \beta_2$, creating a displacement between the spool and sleeve. This displacement corresponds to a change in the area of the valve metering orifices. Therefore, a differential pressure is created across the cylinder.

The operation of the steering system goes as follows: the rotation of the steering wheel with angle β_1 is transmitted to the spool and the upper end of torsion bar. The torsion bar will twist with an angle $\beta = \beta_1 - \beta_2$ resulting in a rotation between the spool and sleeve. This rotation generates a differential pressure across the cylinder. The pressure results in the required control torque by means of the cylinder and piston. The control torque will try to overcome resistant torque from the tires. If the control torque is greater than the resistant torque, the pinion gear rotates with the valve sleeve with angle β_2, i.e. the angle at the lower end of the torsion bar. If the control torque is less than the resistant torque, the pinion gear do not rotate, i.e. $\beta_2 = 0$, and the torsion bar is more twisted and the angle β becomes larger resulting in the increase of the control torque. Therefore, the model with the power steering system may be viewed as a feedback control system.

2.3.2 Power Steering System Model

In Figure 7, only a section of the planar flow paths of the rotary valve is illustrated. The relative angular displacement between the valve spool and sleeve, i.e. β, can be expressed in terms of linear

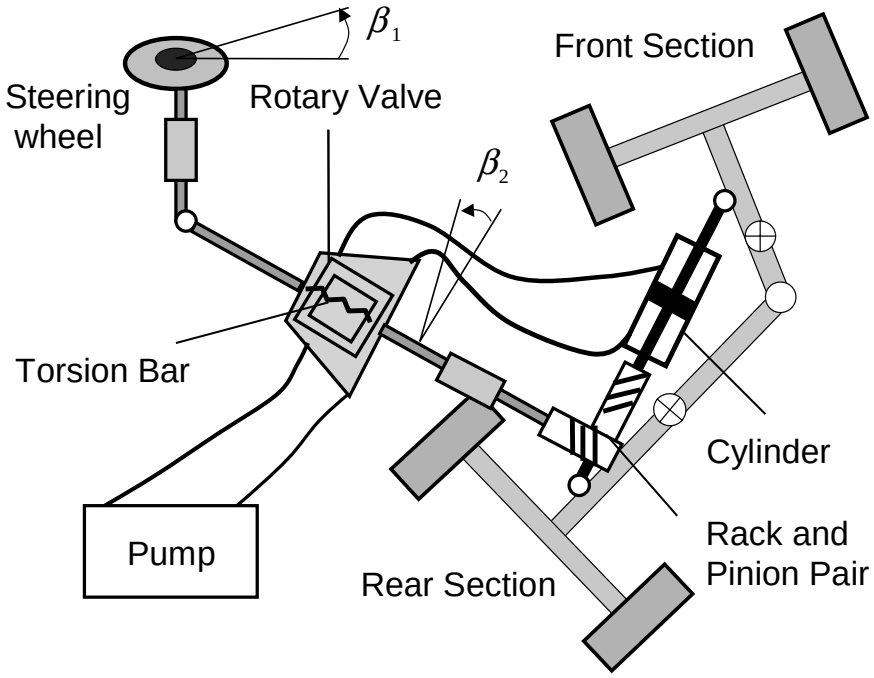

Figure 5: Configuration of the Hybrid Mechanical and Hydraulic Vehicle Model

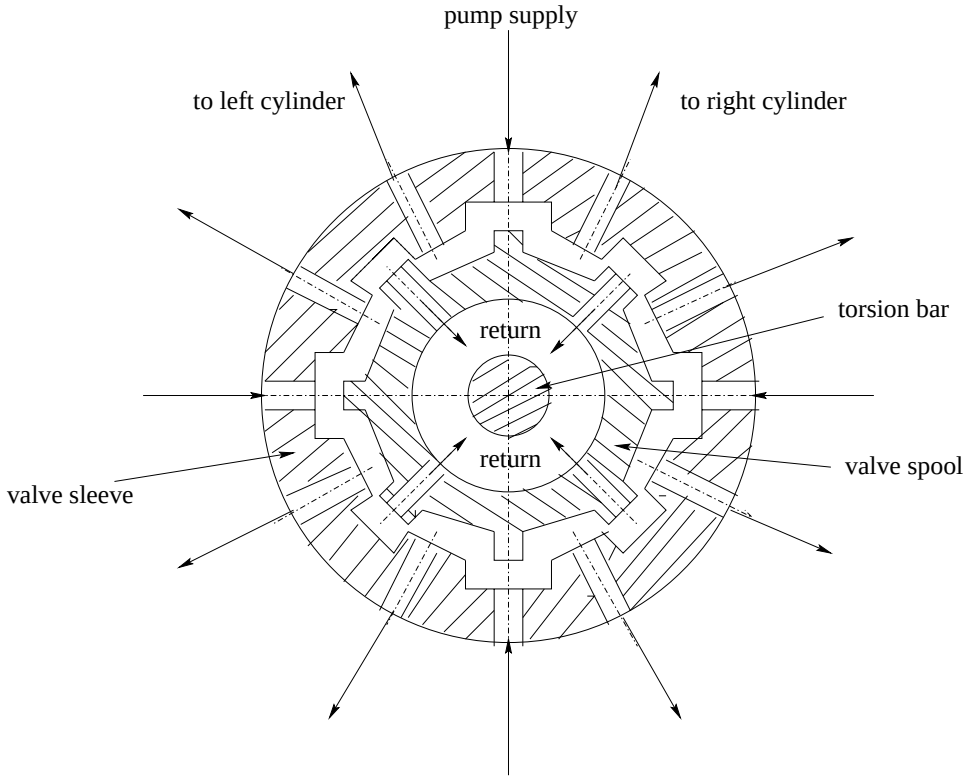

Figure 6: Cross section of rotary valve

displacement n on the inner surface of the sleeve:

$$n = r\beta \tag{19}$$

where r is the radius of the inner sleeve cylinder. The displacement n regulates the metering orifice areas of the rotary valve. Since r is constant, the angular displacement β determines the metering orifice areas of the valve and thus controls the pressure difference across the cylinder.

If the steering input is assumed to be a desired articulated angle ϕ_c, a closed loop control evaluates the difference of ϕ_c with a measured value of ϕ, and this difference is used to regulate β. Hence

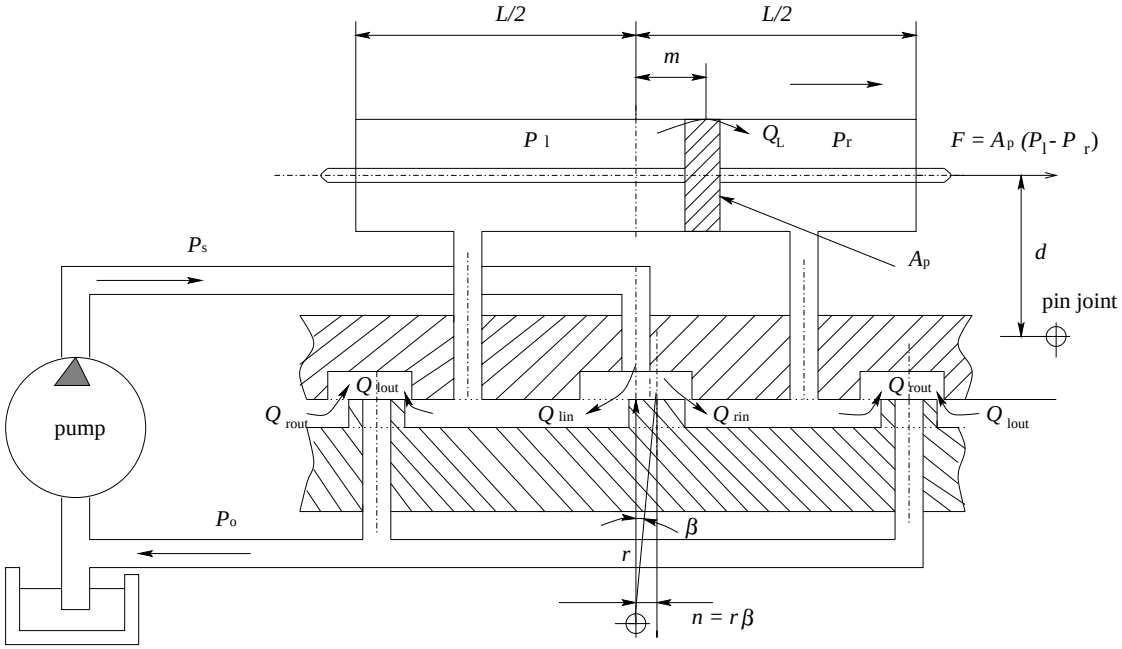

Figure 7: Configuration of power steering system

$$\beta = f(\phi_c - \phi) \tag{20}$$

For small angles of ϕ_c and ϕ, equation (20) may be approximated by the linear function

$$\beta = k_c(\phi_c - \phi) \tag{21}$$

where k_c is a constant. To simplify the modeling, equation (21) is normalised as

$$\overline{\beta} = \overline{\phi}_c - \overline{\phi} \tag{22}$$

where

$$\begin{cases} \overline{\beta} = \beta/\beta_{max} \\ \overline{\phi}_c = \phi_c/\phi_{max} \\ \overline{\phi} = \phi/\phi_{max} \end{cases} \tag{23}$$

where ϕ_{max} is the maximum value of ϕ and $\beta_{max} = k_c\phi_{max}$.

The valve shown in Figure 6 can be modelled as a group of orifices arranged as shown in Figure 8. The orifices without arrows represent fixed holes through the valve body; the orifices with decreasing

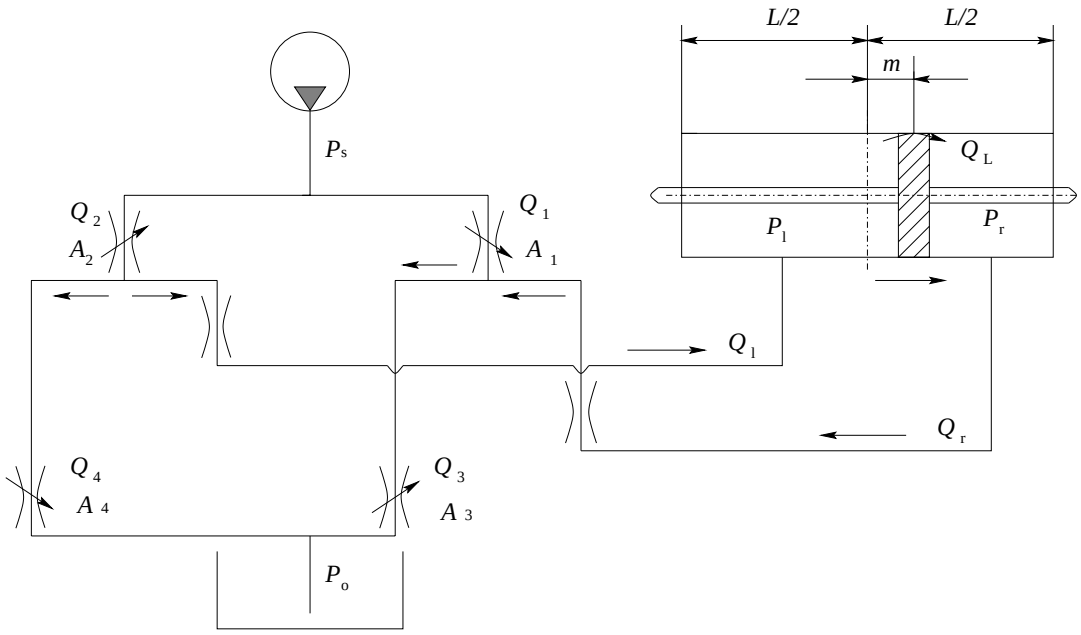

Figure 8: Simplified rotary valve model

arrows represent the orifices that are decreasing in size for a direction of angular displacement β; the orifices with increasing arrows represent the orifices that are getting larger for the same rotation.

In modeling the hydraulic system, the following assumptions were made: there is no pressure drop between the pump and the valve and between the valve and the cylinder; the inertance of the fluid is neglected; the return pressure dynamics are neglected, $P_0 = 0$; the wave dynamics on the fluid transmission lines are neglected; the bulk modulus of the fluid is considered constant.

Based on Figure 8, by applying the orifice equations to the rotary valve metering orifices and the mass conservation equations to the entire hydraulic system, the following equations are obtained:

$$\begin{cases} Q_1 - Q_3 + Q_L = -A_p \frac{dm}{dt} + \frac{A_p(L/2-m)}{B} \frac{dP_r}{dt} \\ Q_2 - Q_4 - Q_L = A_p \frac{dm}{dt} + \frac{A_p(L/2+m)}{B} \frac{dP_l}{dt} \end{cases} \tag{24}$$

where B is the bulk modulus of fluid, and the flow rates Q_i, $i = 1, 2, 3, 4$, and Q_L are defined as

$$\begin{cases} Q_1 = A_1(\beta) C_d \sqrt{\frac{2(P_s - P_r)}{\rho}} \\ Q_2 = A_2(\beta) C_d \sqrt{\frac{2(P_s - P_l)}{\rho}} \\ Q_3 = A_3(\beta) C_d \sqrt{\frac{2P_r}{\rho}} \\ Q_4 = A_4(\beta) C_d \sqrt{\frac{2P_l}{\rho}} \\ Q_L = K_L(P_l - P_r) \end{cases} \tag{25}$$

where ρ is the fluid density, K_L is a constant, and C_d is the flow coefficient for metering orifices. According to the geometric features of the rotary valve, the orifices have the following relations:

$$\begin{cases} A_1(\beta) = A_4(\beta) \\ A_2(\beta) = A_3(\beta) \end{cases} \tag{26}$$

To simplify equation (25), the orifice areas of the rotary valve may be considered as a linear function of the rotary valve rotation angle β. This relation can be described as [15]:

$$\begin{cases} A_1(\beta) = -K_1\beta + l_a \\ A_2(\beta) = K_2\beta + l_a \end{cases} \tag{27}$$

where K_1, K_2, and l_a are constants. Based on equations (25), (26), (27), and Figure 8, we have the following relations:

$$\begin{cases} Q_1 = C_D(-K_1\beta + l_a)(P_s - P_r)^{1/2} \\ Q_2 = C_D(K_2\beta + l_a)(P_s - P_l)^{1/2} \\ Q_3 = C_D(K_2\beta + l_a)P_r^{1/2} \\ Q_4 = C_D(-K_1\beta + l_a)P_l^{1/2} \\ C_D = C_d\sqrt{2/\rho} \\ Q_l = Q_2 - Q_4 \\ Q_r = Q_3 - Q_1 \\ V_m = \int_0^t Q_l dt = \int_0^t Q_r dt \end{cases} \tag{28}$$

Assuming

$$Q = (Q_l + Q_r)/2 \tag{29}$$

with the normalization of equation (29), we have

$$\overline{Q} = (\overline{Q}_l + \overline{Q}_r)/2 \tag{30}$$

where

$$\begin{cases} \overline{Q} = Q/Q_{max} \\ \overline{Q}_l = Q_l/Q_{max} \\ \overline{Q}_r = Q_r/Q_{max} \\ Q_{max} = C_D K_3 \beta_{max} P_s^{1/2} \end{cases} \tag{31}$$

and K_3 is a constant. Assuming

$$\dot{\overline{V}}_m = \frac{\dot{V}_m}{V_{m0}} = \frac{Q_{max}}{V_{m0}}\overline{Q} \tag{32}$$

In terms of perturbations, equations (30) and (32) become

$$\begin{cases} \overline{q} = (\overline{q}_l + \overline{q}_r)/2 \\ \dot{\overline{v}}_m = \frac{Q_{max}}{V_{m0}}\overline{q} \end{cases} \tag{33}$$

Note that q, q_r, q_l, and v_m represent perturbations of the corresponding upper case variables.

To linearize equation (24), Q_i may be expanded to first order about $\beta = 0$, and $P_l = P_r = P_s/2$. Thus

$$\begin{cases} \Delta Q_1 = -C_D K_1 (P_s/2)^{1/2}\Delta\beta - \frac{1}{2}C_D l_a (P_s/2)^{-1/2}\Delta P_r \\ \Delta Q_2 = C_D K_2 (P_s/2)^{1/2}\Delta\beta - \frac{1}{2}C_D l_a (P_s/2)^{-1/2}\Delta P_l \\ \Delta Q_3 = C_D K_2 (P_s/2)^{1/2}\Delta\beta + \frac{1}{2}C_D l_a (P_s/2)^{-1/2}\Delta P_r \\ \Delta Q_4 = -C_D K_1 (P_s/2)^{1/2}\Delta\beta + \frac{1}{2}C_D l_a (P_s/2)^{-1/2}\Delta P_l \end{cases} \tag{34}$$

Based on equations (28), we have

$$\Delta Q_l + \Delta Q_r = \Delta Q_2 + \Delta Q_3 - (\Delta Q_1 + \Delta Q_4) \tag{35}$$

Substitution of equation (34) into equation (35) results in

$$\frac{1}{2}(\Delta Q_l + \Delta Q_r) = C_D(P_s/2)^{1/2}(K_1 + K_2)\Delta\beta - \frac{1}{2}C_D l_a(P_s/2)^{-1/2}(\Delta P_l - \Delta P_r) \tag{36}$$

Normalizing equation (36), we have

$$\frac{1}{2}(\Delta Q_l + \Delta Q_r)/Q_{max} = \frac{1}{2}\sqrt{2}(\frac{K_1 + K_2}{K_3}\frac{\Delta\beta}{\beta_{max}} - \frac{l_a}{K_3\beta_{max}}(\frac{\Delta P_l}{P_s} - \frac{\Delta P_r}{P_s})) \tag{37}$$

which may be rewritten as

$$\overline{q} = k_0\overline{\beta}_m - l_0\Delta\overline{p} \tag{38}$$

where

$$\begin{cases} k_0 = \frac{1}{2}\sqrt{2}\frac{K_1+K_2}{K_3} \\ l_0 = \frac{1}{2}\sqrt{2}\frac{l_a}{K_3\beta_{max}} \\ \overline{\beta}_m = \frac{\Delta\beta}{\beta_{max}} \\ \Delta\overline{p} = \frac{\Delta P_l}{P_s} - \frac{\Delta P_r}{P_s} \end{cases} \tag{39}$$

With equations (24) and (28), we have the following linear equation

$$\overline{Q} = \frac{A_p\dot{\phi}d}{Q_{max}} + \frac{V_{m0}P_s}{2BQ_{max}}\frac{(\dot{P}_l - \dot{P}_r)}{P_s} + \frac{K_L P_s}{Q_{max}}\frac{(P_l - P_r)}{P_s} \tag{40}$$

To linearize equation (40), the following assumptions are made:

$$\begin{cases} \dot{m} = \dot{\phi}d \\ V_l = A_p(L/2 + m) \\ V_r = A_p(L/2 - m) \end{cases} \tag{41}$$

and V_l and V_r remain close to V_{m0}.

In terms of perturbations, equation (40) becomes

$$\overline{q} = \frac{A_p d}{Q_{max}}\dot{\phi} + \frac{V_{m0}P_s}{2BQ_{max}}\Delta\dot{\overline{p}} + K_{L0}\Delta\overline{p} \tag{42}$$

where $K_{L0} = K_L P_s/Q_{max}$.

Combining equations (33), (38), and (42), we have the following governing equations describing the hydraulic steering system:

$$\begin{cases} \frac{V_{m0}}{Q_{max}}\dot{\overline{v}}_m = k_0\overline{\beta} - l_0\Delta\overline{p} \\ \frac{V_{m0}P_s}{2BQ_{max}}\Delta\dot{\overline{p}} + \frac{A_p d}{Q_{max}}\dot{\phi} = -(l_0 + K_{L0})\Delta\bar{p} + k_0\overline{\beta} \end{cases} \tag{43}$$

where for small perturbation of β, $\overline{\beta}_m = \overline{\beta}$.

As shown in Figure 7, the hydraulic cylinder actuator force and torque are as follows:

$$\begin{cases} F = A_p(P_l - P_r) = A_p P_s\Delta\overline{p} \\ T_N = A_p P_s\Delta\overline{p}d \end{cases} \tag{44}$$

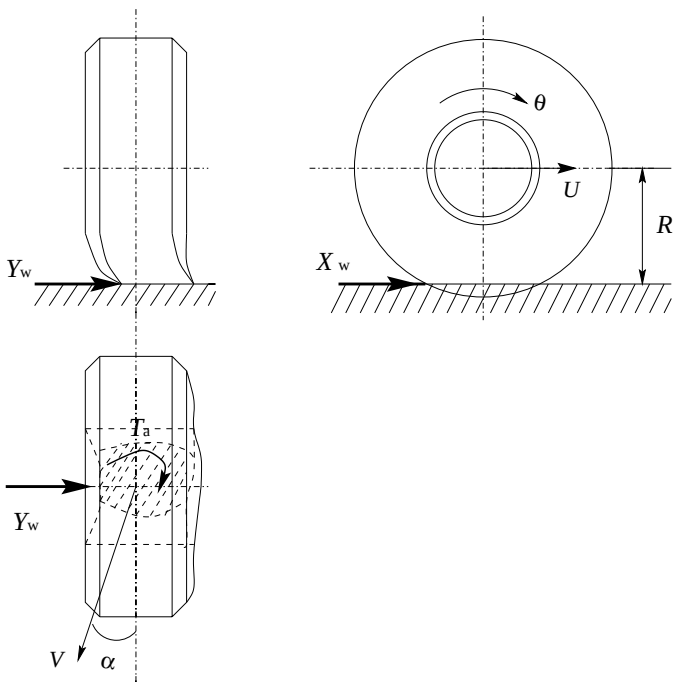

Figure 9: Dynamic tire model

2.3.3 Tire Model

Figure 9 shows the dynamic tire model used in the articulated frame steer vehicle model. A detailed derivation of this tire model was offered by Horton and Crolla [3]. The governing equations of the tire model are:

$$\begin{cases} \frac{\sigma_x R}{u_1}\Delta\dot{\mathbf{X}}_i + \Delta\mathbf{X}_i = -C_{Xi}(R\Delta\omega_i + 2t_a\gamma_i)/u_1 \\ I_w\Delta\dot{\omega}_i = R\Delta\mathbf{X}_i \\ \frac{\sigma_y R}{u_1}\dot{Y}_i + Y_i = -C_{Yi}\alpha_i \\ \frac{\sigma_t R}{u_1}\dot{T}_{ai} + T_{ai} = C_{Ti}\alpha_i \end{cases} \tag{45}$$

where $i = 1, 2$, denote front or rear axle of the vehicle, γ_i is the yaw rate of front or rear section of the vehicle, u_1 is the longitudinal velocity of the front section of the vehicle, $\Delta\mathbf{X}_i$ and Y_i are defined in equations (8) and (10), T_{ai} are defined as

$$\begin{cases} T_{a1} = T_{w1} + T_{w2} \\ T_{a2} = T_{w3} + T_{w4} \end{cases} \tag{46}$$

where T_{wj}, $j = 1, 2, 3, 4$, is the aligning torque on each tire. For small slip angle α_i, $i = 1, 2, 3, 4$, ω_i, $\Delta\omega_1$ and $\Delta\omega_2$ are defined as

$$\begin{cases} \omega_i = \dot{\theta}_i + U_i/R \\ \Delta\omega_1 = \omega_1 - \omega_2 \\ \Delta\omega_2 = \omega_3 - \omega_4 \end{cases} \tag{47}$$

where θ_i and U_i denote the spin angle and longitudinal speed of wheel i. In equation (45), C_{Xi} and C_{Yi} are defined as follows:

$$\begin{cases} C_{Xi} = C_{xi}Z_i \\ C_{Ti} = C_{ti}Z_i \end{cases} \tag{48}$$

where the definitions of C_{xi}, C_{ti} and all other symbols in equation (45) are offered in the Nomenclature.

2.3.4 Hybrid Vehicle Model

The integration of the 3 DOF model described in equation (18), the hydraulic power steering system described in equation (43), and the tire model described in equation (45) results in the hybrid vehicle model that can be described by the equations of motion in state-space form as:

$$\mathbf{A}\dot{\mathbf{r}} = \mathbf{B}\mathbf{r} + \mathbf{C}\phi_c \tag{49}$$

where the state variable vector $\mathbf{r}$ is:

$$\mathbf{r} = \begin{bmatrix} v_1 & \gamma_1 & \gamma_2 & \phi & Y_1 & Y_2 & \Delta\bar{p} & \Delta\bar{v}_m & T_{a1} & T_{a2} & \Delta X_1 & \Delta X_2 & \Delta\omega_1 & \Delta\omega_2 \end{bmatrix}^T \tag{50}$$

and ϕ_c is the desired articulated angle. The system matrices $\mathbf{A}$, $\mathbf{B}$, and $\mathbf{C}$ are given in the Appendix.

Notice that in the hybrid vehicle model, the lateral tire forces Y_i are determined by equation (45) instead of equation (3) and the internal torques T_1 and T_2 are offered by:

$$\begin{cases} T_1 = -A_p dP_s \Delta\bar{p} \\ T_2 = A_p dP_s \Delta\bar{p} \end{cases} \tag{51}$$

Figure 10 shows the block diagram of the linearized hybrid vehicle model.

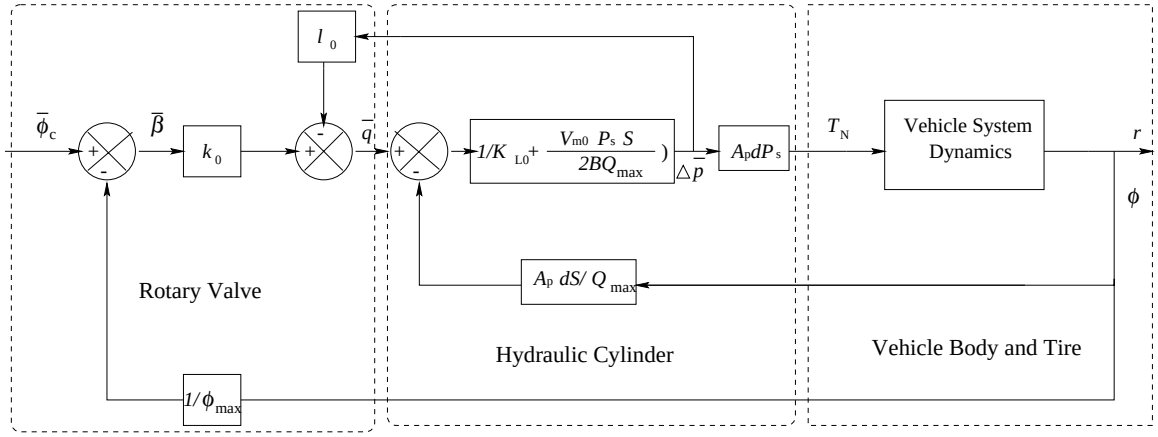

Figure 10: Block diagram for the hybrid vehicle model (S denotes the Laplace operator)

3 Results and Discussion

From equations (4), (18), and (49), we may obtain the system matrix $\mathbf{A}^{-1}\mathbf{B}$ for the 2 DOF, 3 DOF, and hybrid vehicle models, respectively. Based on the eigenvalue analysis of the system matrix, we may investigate the lateral stability of the corresponding vehicle model; we may also find the natural frequencies and mode shapes for the model concerned. If the real parts of the eigenvalues are positive, the motion modes corresponding to the eigenvectors are unstable.

In this section, eigenvalue analyses are presented by means of plots in which the relationships between the real parts of eigenvalues and the forward speed of the articulated vehicle are offered.

3.1 Comparison of Different Vehicle Models

In this subsection, the relationship between the "oversteer" and "jack-knife" motion modes is disclosed and the effects of selected design variables on the stability of the vehicle are discussed.

3.1.1 Comparison of 2 DOF and 3 DOF models

Figure 11 shows the steady state steering behavior of the 2 DOF model when C_{y1} and C_{y2} take different values. Like the conventional "bicycle model" for vehicles with Ackerman steering mechanisms, the 2 DOF model for the articulated vehicles has three characteristics: understeer (curve 3), neutral steer (curve 2), and oversteer (curve 1). In the oversteer case, the critical speed is $14.7\ [m/s]$.

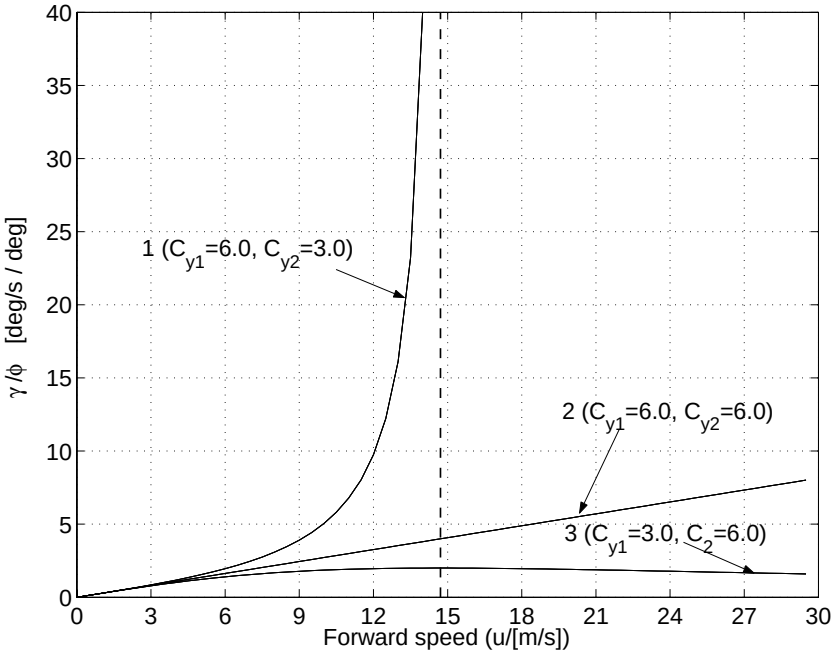

Figure 11: Steady state steering behavior of the 2 DOF model

For the oversteer case, the real parts of eigenvalues are plotted against forward speed as shown in Figure 12. There are two motion modes: oversteer mode and lateral motion mode. Note that the oversteer mode and lateral motion mode correspond to the yaw and lateral motions of the 2 DOF model, respectively. The oversteer mode dominates the stability of the model and the critical speed is $14.7\ [m/s]$.

For the 3 DOF model, with $C_{y1} = 6.0, C_{y2} = 3.0$, for $K_\phi = 2 \times 10^8\ [Nm/rad]$ and $K_\phi = 2 \times 10^5\ [Nm/rad]$, the motion modes are illustrated in Figure 13and Figure 14, respectively. In Figure 13, three motion modes, oversteer mode, lateral motion mode, and oscillatory mode, are plotted. Similar to the 2 DOF model, the oversteer mode and lateral motion mode correspond to the yaw and lateral motions of front section of the 3 DOF model, respectively. The oscillatory mode corresponds to the yaw motion of the rear section of the 3DOF model. The oversteer mode dominates the stability of the vehicle and the critical speed is $14.7\ [m/s]$. In Figure 14, three motion modes, jack-knife, swing, and snaking, are also plotted. These motion modes are similar to the counterparts identified

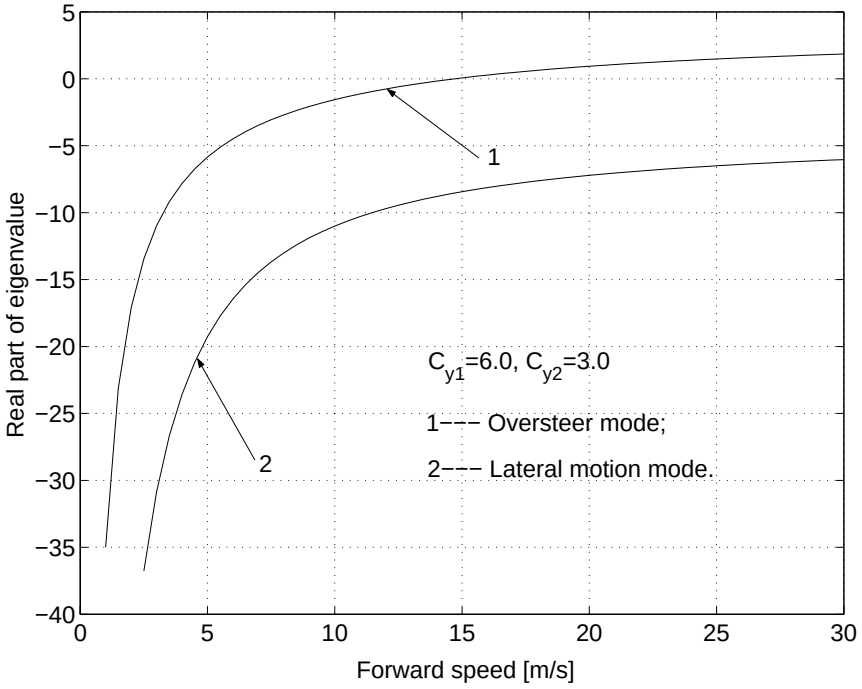

Figure 12: Real parts of eigenvalues versus forward speed (2 DOF model, $C_{y1} = 6.0, C_{y2} = 3.0$)

in conventional articulated vehicles. In this case, the jack-knife mode determines the critical speed and it takes the value of $7.9\ [m/s]$. Comparing Figure 14 with Figure 13, we conclude that as K_ϕ decreases, the corresponding mode shape changes and the critical speed decreases.

To investigate the effects of K_ϕ on the stability of the 3 DOF model, for different values of K_ϕ, the corresponding "oversteer" or "jack-knife" modes together with the oversteer mode of the 2 DOF model are plotted in Figure 15. As expected, with the increase of K_ϕ, the "oversteer" mode of the 3 DOF becomes closer to the corresponding mode of the 2 DOF model and the critical speed increases. This observation is consistant with that found by Horton and Crolla [3].

To examine the "oversteer" mode shape of the 3 DOF model, when K_ϕ is assigned $2\times10^8\ [Nm/rad]$ and $2 \times 10^5\ [Nm/rad]$, the time response of the yaw angle of the front and rear section of the model, as well as the articulated angle, are offered in Figures 16 and 17, respectively. Note that, to obtain the time responses including ϕ_1 and ϕ_2, the governing equations of motion described in equation (18) should be modified and the augmented state variable vector becomes $\mathbf{r} = [v_1\ \gamma_1\ \gamma_2\ \phi\ \phi_1\ \phi_2]^T$. The initial conditions are listed in Figures 16 and 17. To obtain the time responses, the forward vehicle speed was set to the value of $15.0[m/s]$, slightly above the critical speed. As shown in Figure 16, after the initial excitation, ϕ, ϕ_1, and ϕ_2 oscillate with high frequencies and as time processes, ϕ_1 and ϕ_2 become identical and ϕ approaches to zero. In contrast with Figure 16, Figure 17 shows that after the initial perturbation, ϕ, ϕ_1, and ϕ_2 do not oscillate and as time goes, ϕ_1 and ϕ_2 diverge and ϕ becomes larger. Thus, as K_ϕ decreases, the mode concerned will change from oversteer mode of the 2 DOf model to the jack-knife mode of the 3 DOF model and the corresponding critical speed decreases.

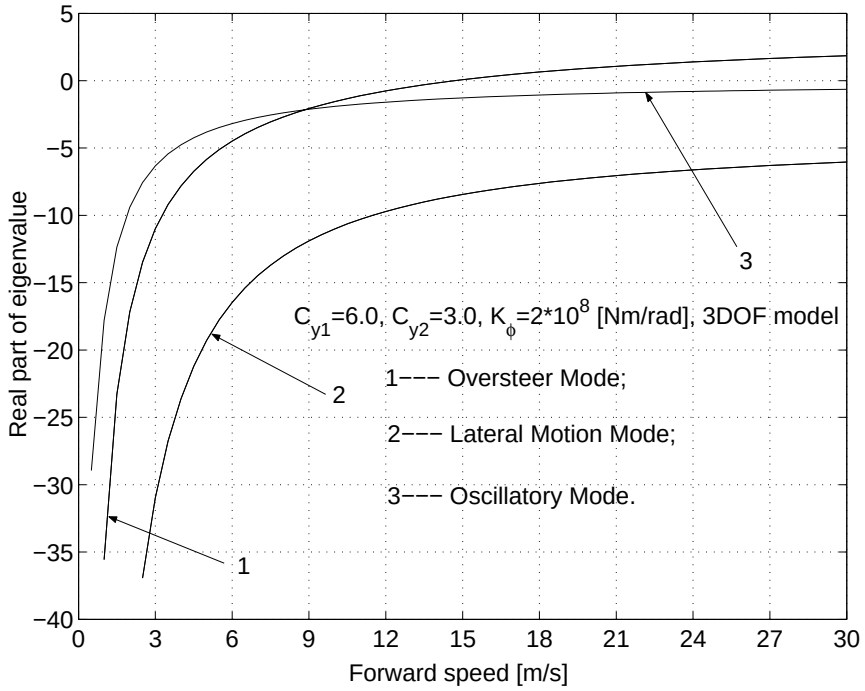

Figure 13: Real parts of eigenvalues versus forward speed (3 DOF model, $C_{y1} = 6.0, C_{y2} = 3.0, K_\phi = 2 \times 10^8\ [Nm/rad]$)

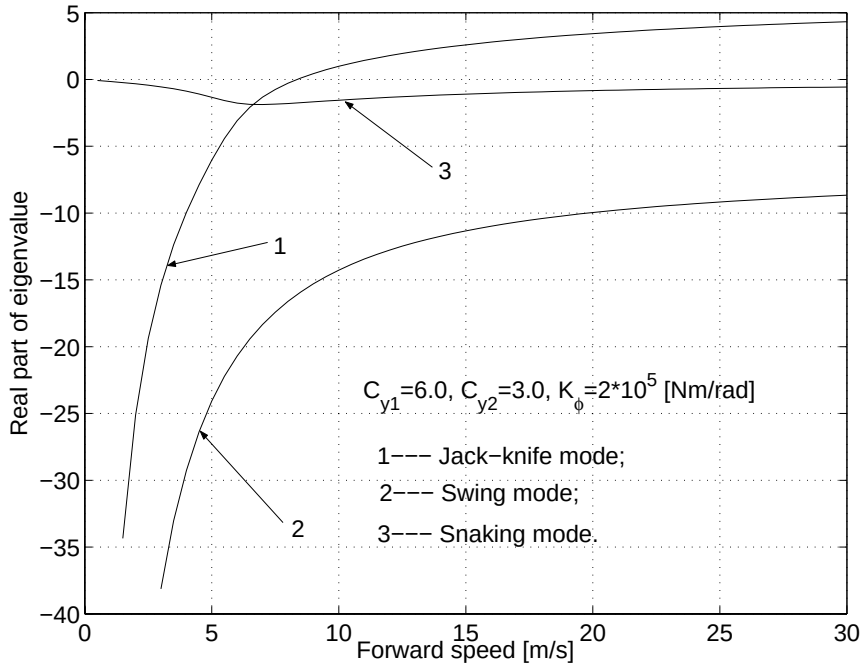

Figure 14: Real parts of eigenvalues versus forward speed (3 DOF model, $C_{y1} = 6.0, C_{y2} = 3.0, K_\phi = 2 \times 10^5\ [Nm/rad]$)

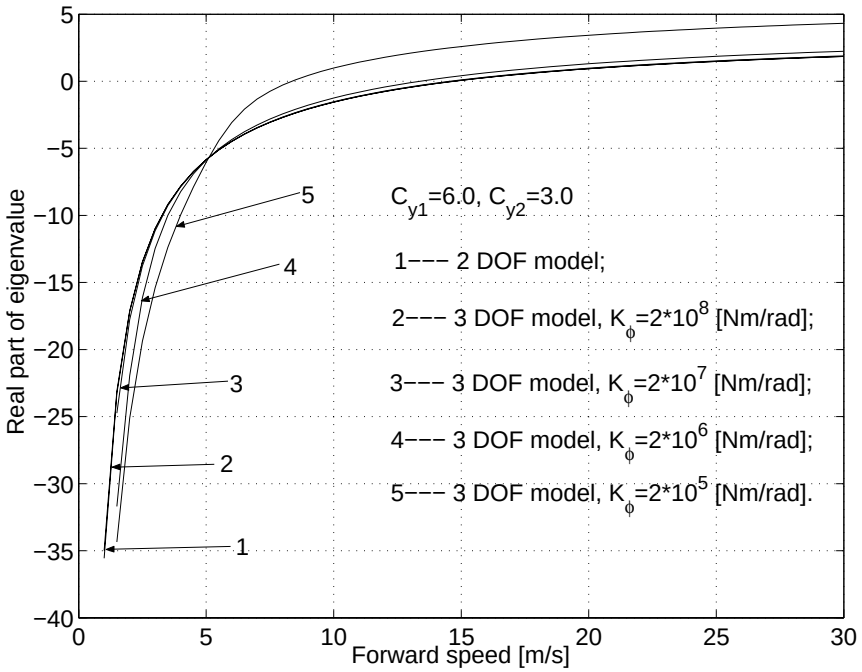

Figure 15: Effects of K_ϕ on the vehicle stability (3 DOF model, $C_{y1} = 6.0, C_{y2} = 3.0$)

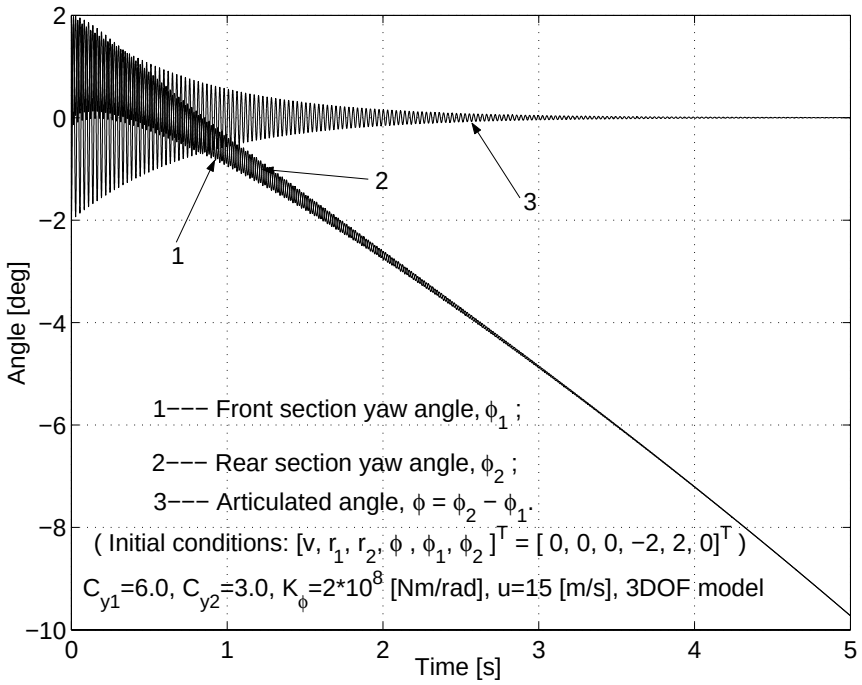

Figure 16: Time responses of articulated angle and the front and rear section yaw angles (3 DOF model, $K_\phi = 2 \times 10^8\ [Nm/rad]$)

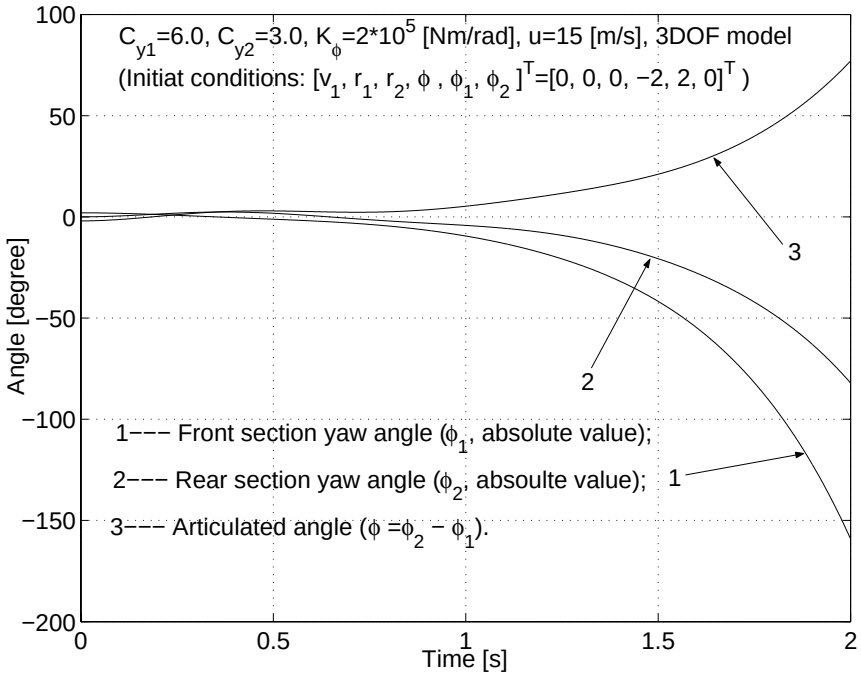

Figure 17: Time responses of articulated angle and the front and rear section yaw angles (3 DOF model, $K_\phi = 2 \times 10^5\ [Nm/rad]$)

3.1.2 Comparison of 3 DOF and higher order models

To investigate the effects of the dynamic tire model, the lateral tire forces in particular, on the stability of the vehicle, equation (49) is reduced to a 6^{th} order model, i.e. only 6 state variables are considered ($\mathbf{r} = [v_1\ \gamma_1\ \gamma_2\ \phi\ \mathbf{Y}_1\ \mathbf{Y}_2]^T$). When the relaxation length for tire lateral motion σ_y (see equation (45)) takes different values, the corresponding "oversteer" modes of this model are offered in Figure 18 and these modes are compared with that of the 3 DOF model. Observation of the motion modes shown in Figure 18 reveals that, over the higher speed range, the motion mode is independent of σ_y. However, over the lower speed range, as the value of σ_y increases, the motion mode diverges from that of the 3 DOF model. This phenomenon may be interpreted by the fact that as vehicle forward speed increases, the transient potion of the lateral force decays quickly and the dynamic lateral force becomes closer to the steady state lateral force. This is also the case when σ_y takes smaller values. However, over the lower forward speed range, if σ_y takes larger values, the larger dynamic transient lateral force degrades the stability of the motion mode.

To investigate the effect of hydraulic steering system on the stability of the vehicle, the previous 6^{th} order model is augmented to 8^{th} order ($\mathbf{r} = [v_1\ \gamma_1\ \gamma_2\ \phi\ \mathbf{Y}_1\ \mathbf{Y}_2\ \Delta\overline{p}\ \overline{v}_m]^T$). For different values of the valve zero displacement leakage coefficient l_0, the corresponding "oversteer" mode is plotted in Figure 19. For comparison, the counterpart of the 6^{th} order model is also illustrated. Without leakage, the mode shape of the 8^{th} order model is the same as that of the 6^{th} order model. However, the introduction of leakage of the valve at zero displacement results in an unstable "oversteer" mode over the whole range of speed. As described previously, with the introduction of leakage of the valve, the equivalent angular spring stiffness about the pin joint decreases and the oversteer mode will switch to the jack-knife mode. Hence, the above phenomenon is consistent with the observation

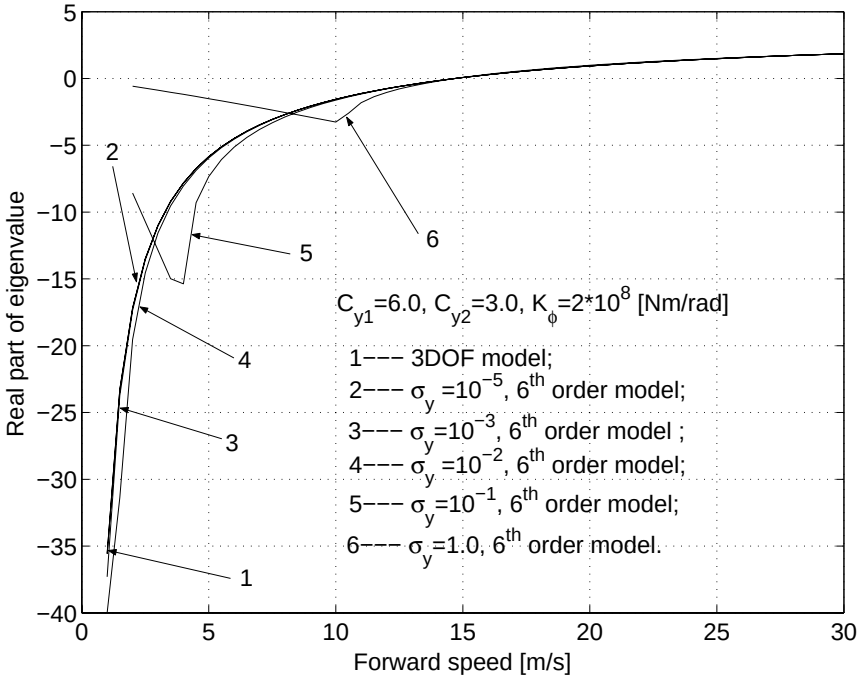

Figure 18: Effects of dynamic tyre model on the stability of the vehicle (6^{th} order model, $C_{y1} = 6.0, C_{y2} = 3.0, K_\phi = 2 \times 10^8\ [Nm/rad]$)

by Horton and Crolla [3] that "The frame steer configuration is inherently unstable and exhibits a tendency to jack-knife about the articulation point at any speed".

To find the difference between the 8^{th} order model and the 14^{th} order model, i.e., in equation (49), the state variable vector $\mathbf{r}$ takes the form as expressed in equation (50) and the variable set, i.e. σ_x, σ_t, and I_w (see equation (45)), takes two set of values as listed in Figure 20. For each set of values, the corresponding "oversteer" mode is presented together with the counterpart of the 8^{th} order model. As shown in Figure 20, the longitudinal tyre forces and aligning torques have a small effect on the stability of the vehicle.

3.2 Parameter Study

In this subsection, two cases are studied. In the first case, $C_{y1} = 6.0$, $C_{y2} = 3.0$, and the other parameters take their nominal values listed in Table 2. Since for the 2 DOF model, when C_{y1} and C_{y2} take the above values, the vehicle model has oversteer steady state steering behaviour, we call this the "oversteer case". In the second case, $C_{y1} = 6.0$, $C_{y2} = 6.0$, and the other parameters still take their nominal values. Similarly, we call this the "neutral steer case". In both cases, based on the hybrid vehicle model described in equation (49), the relationship between the stability of the vehicle and the variation of the hydraulic cylinder leakage constant K_{L0} is investigated.

3.2.1 Oversteer Case

Figure 21 shows the "oversteer" modes, when K_{l0} takes the values of 0.0, 0.001, 0.01, and 0.1. Comparing Figure 21 with Figure 19, we observe that for both cases the mode shapes are very

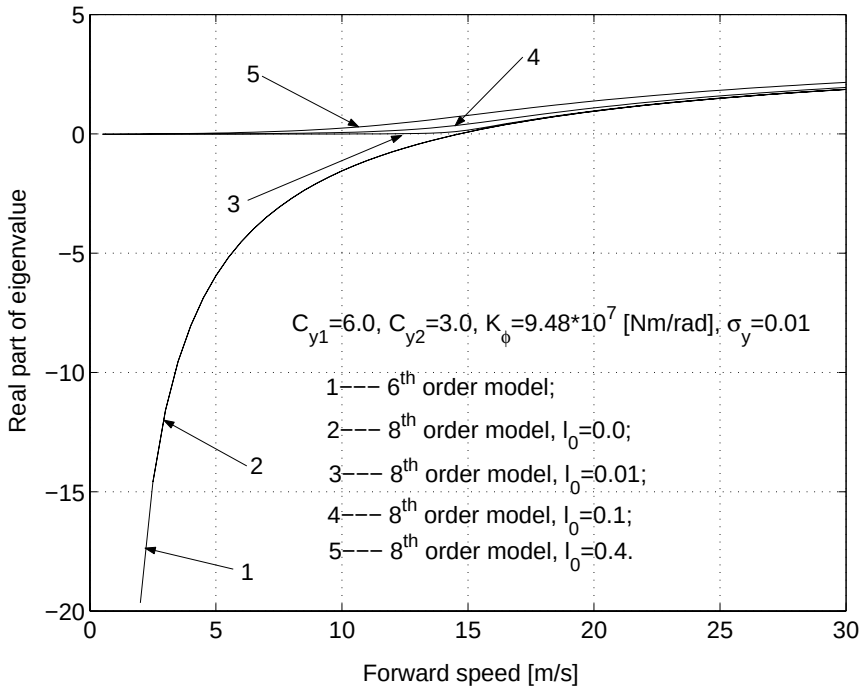

Figure 19: Effects of hydraulic system on the stability of the vehicle (6^{th} and 8^{th} order models, $C_{y1} = 6.0, C_{y2} = 3.0, K_\phi = 9.48 \times 10^8\ [Nm/rad], \sigma_y = 0.01$)

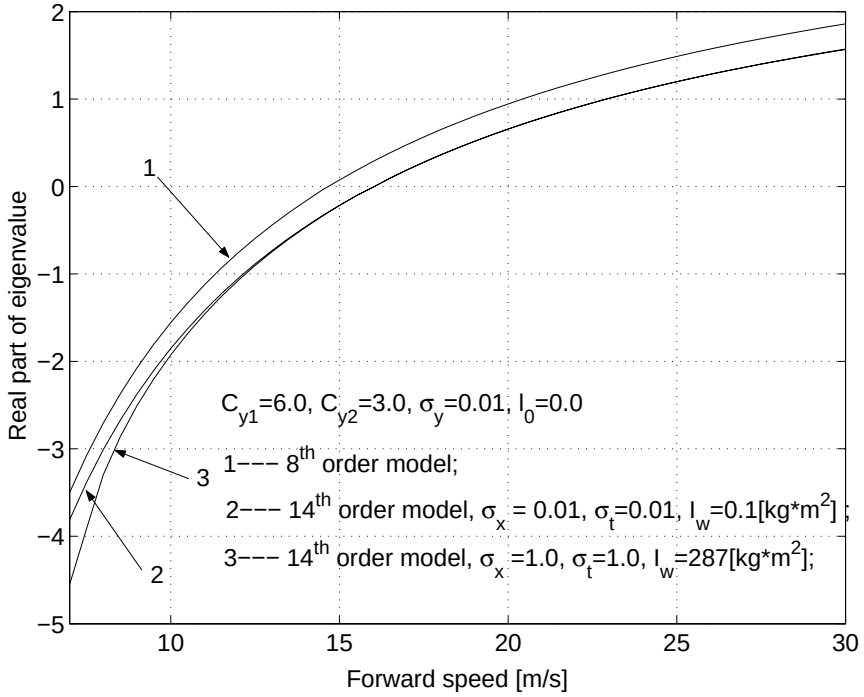

Figure 20: Effects of longitudinal tyre forces and aligning torques on the stability of the vehicle (8^{th} and 14^{th} order models, $C_{y1} = 6.0, C_{y2} = 3.0, K_\phi = 9.48 \times 10^8\ [Nm/rad], \sigma_y = 0.01, l_0 = 0.0$)

similar. Thus, we may conclude that without fluid leakage in hydraulic power steering system, the mode concerned is very close to the oversteer mode of the corresponding 2 DOF rigid vehicle model. However, with fluid leakage in either the rotary valve or the hydraulic cylinder, the mode concerned is unstable over the whole range of forward speed.

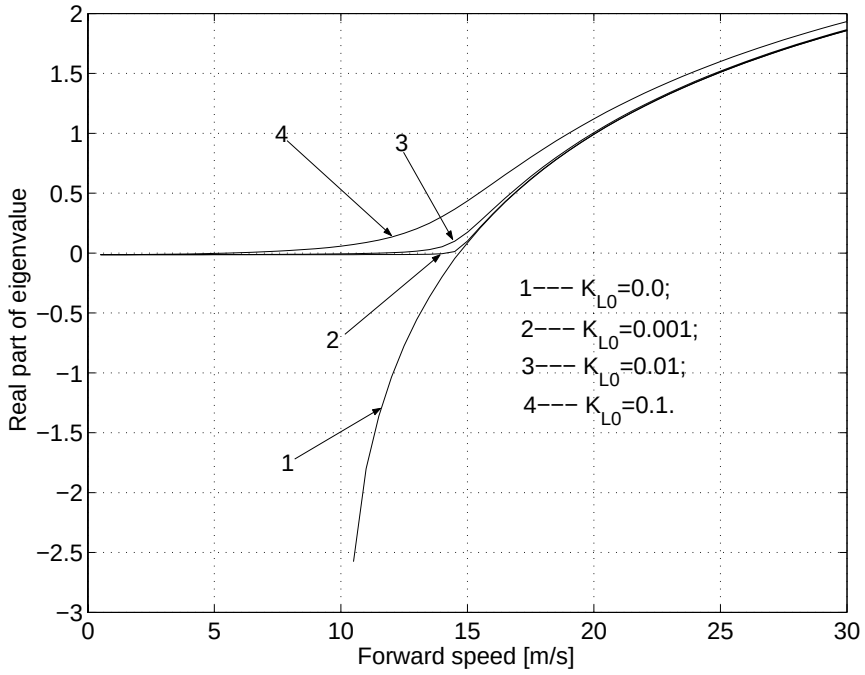

Figure 21: Effect of K_{L0} variation on the stability of the oversteered vehicle

3.2.2 Neutral Steer Case

Figure 22 illustrates the 7 least damped motion modes when $K_{L0} = 0.0$. Mode 1 corresponds to the snaking mode that oscillates with natural frequency of $25.0\ Hz$. Over the speed range of interest, the snaking mode has a damping ratio that is very close to zero. Notice that, during the numerical simulations, we found that when $C_{y1} = 3.0$, $C_{y1} = 6.0$, and all other parameters take their nominal values, the corresponding snaking mode has positive damping ratio over the speed range concerned.

Figure 23 shows the 7 least damped motion modes when K_{L0} takes the value of 0.01. Compared with Figure 22, Figure 23 reveals the fact that as K_{L0} increases, the stability margin of the snaking mode increases. Thus, in contrast with the oversteer case, in natural steer (or understeer case), the introduction of fluid leakage either in the hydraulic cylinder or the rotary valve may result in improved stability of the snaking mode.

4 Conclusions

To investigate the lateral stability of articulated frame steering vehicles, a 2 degrees of freedom (DOF) "bicycle model", a 3 DOF model, and a hybrid model, including a hydraulic power steering sub-model, dynamic tire sub-model, and mechanical vehicle sub-model, are generated. To reveal

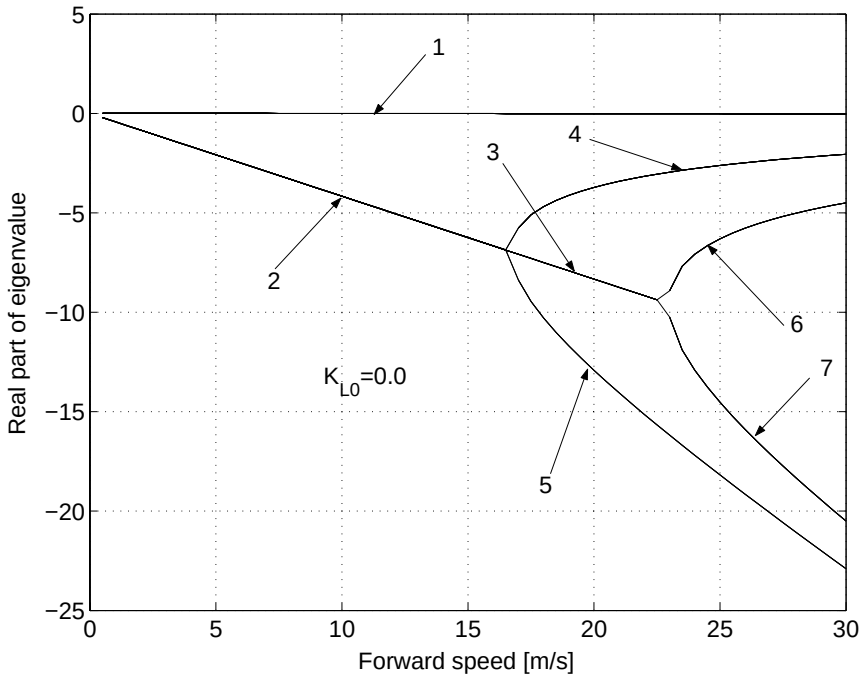

Figure 22: Real part of eigenvalue against forward speed ($K_{L0} = 0.0$)

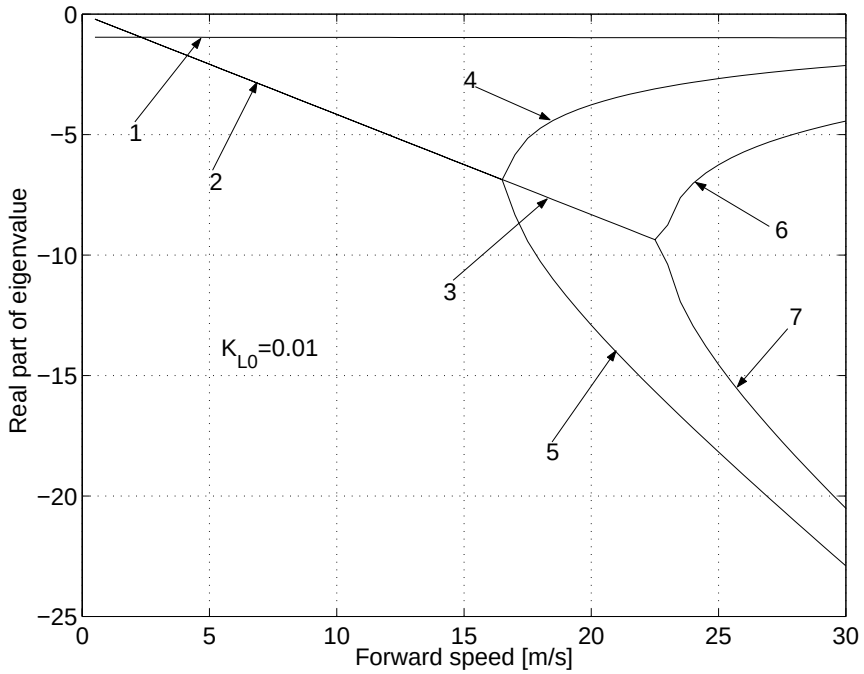

Figure 23: Real part of eigenvalue against forward speed ($K_{L0} = 0.01$)

the relationship between the "oversteer" and "jack-knife" motion modes and investigate the effects of design variables on the stability of the vehicles, the numerical simulation results based on the 2 DOF, 3 DOF, and hybrid vehicle models are compared and discussed. Although the 2 DOF rigid vehicle model is simple, it can be used as a reference model to interpret the numerical results based on complex models that are computationally expensive.

Numerical results reveal that if the equivalent angular spring (representing the hydraulic cylinder between the front and rear sections of the articulated frame steering vehicle) becomes soft, the critical speed decreases; in the cases of "oversteer" mode dominant motion, as the spring stiffness decreases, the oversteer mode evolves into a jack-knife mode. Compared with the static tire model, the effects of dynamic tire model degrades the stability of the vehicle model over the lower speed range. Numerical results also show that in the case of "snaking" mode dominant motion, the introduction of fluid leakage in hydraulic power steering system results in the improvement of the lateral stability of the vehicles. However, in the case of "oversteer" mode dominant motion, the introduction of fluid leakage degrades the stability of the corresponding jack-knife mode, which is unstable over the whole range of forward speed.

Acknowledgment

Financial support of this research by Materials and Manufacturing Ontario and by Timberjack (a John Deere Company) is gratefully acknowledged.

References

[1] Scholl, R., and Klein, R, "Stability Analysis of an Articulated Vehicle Steering System", *Earth-moving Industry Conference*, Illinois, SAE Paper 710527, 1971.

[2] Crolla, D., and Horton, D., "The Steering Behaviour of Articulated Body Steer Vehicles", *I. Mech. E. Conference on Road Vehicle Handling*, MIRA, Nuneaton, Paper C123/83, 139-146, 1983.

[3] Horton, D., and Crolla, D., "Theoretical Analysis of the Steering Behaviour of Articulated Frame Steer Vehicles", *Vehicle System Dynamics* **15**, 211-234, 1986.

[4] Vlk, F., "Handling Performance of Truck-Trailer Vehicles: A State-of-the-Art Survey", *Int. J. of Vehicle Design* **6(3)**, 323-361, 1985.

[5] Mooring, B., and Genin, J., "A Kinematic Constraint Method for Stability Analysis of Articulated Vehicles", *Int. J. of Vehicle Design* **3(2)**, 190-201, 1982.

[6] Nalecz, A., and Genin, J., "Dynamic Stability of Heavy Articulated Vehicles", *Int. J. of Vehicle Design* **5(4)**, 417-426, 1984.

[7] Anderson, R., Elkins, J., and Brickle, B., "Rail Vehicle Dynamics for the 21^{th} Century", *Proceedings of ICTAM'2000*, Chicago, USA, 2001.

[8] Knothe, K., and Böhm, F., "History of Stability of Railway and Road Vehicles", *Vehicle System Dynamics* **31**, 283-323, 1999.

[9] Jindra, F., “Tractor and Semitrailer Handling”, *Automobile Engineer* **55(2)**, 60-69, 1965.

[10] Vlk, F., “Lateral Stability of Articulated Buses”, *Int. J. of Vehicle Design* **9(1)**, 35-51, 1988.

[11] He, Y., and McPhee, J., “Optimization of the Lateral Stability of Rail Vehicles”, *Vehicle System Dynamics* **38**, 361-390, 2002.

[12] Yu, Z., “Theory of Automobiles”, Publishing House of the Mechanical Industry, Beijing, China, (in Chinese), 1989.

[13] Ellis, J., “Vehicle Dynamics”, Business Books, Ltd., London, 1969.

[14] Proca, A., and Keyhani, A., “Identification of Power Steering System Dynamic Models”, *Mechatronics* **8**, 255-270, 1998.

[15] Birsching, J., “Two Dimensional Modeling of a Rotary Power Steering Valve”, *SAE Technical Paper 1999-01-0396*, 1-5, 1999

[16] McCloy, D., and Martin, H., “Control of Fluid Power: Analysis and Design”, $2nd$ (Revised) Edition, Chichester, England: Ellis Horwood Limited, 1980.

[17] Gillespie, T., “Fundamentials of Vehicle Dynamics”, SAE, Warrendale, PA, 1992.

Appendix

1 System Matrices for the 2 DOF Vehicle Model

$$\mathbf{A} = \begin{bmatrix} (m_1+m_2)u & -m_2(b+e)u \\ -m_2(b+e)u & (I_1+I_2+m_2(b^2+e^2+2be))u \end{bmatrix} \tag{52}$$

$$\mathbf{B} = \begin{bmatrix} C_{Y1}+C_{Y2} & aC_{Y1}-m_1u^2-m_2u^2-(b+L_2)C_{Y2} \\ aC_{Y1}-C_{Y2}(b+L_2) & a^2C_{Y1}+C_{Y2}(b+L_2)^2+m_2u^2(b+e) \end{bmatrix} \tag{53}$$

$$\mathbf{C} = \begin{bmatrix} uC_{Y2} \\ -uC_{Y2}(b+L_2) \end{bmatrix} \tag{54}$$

2 System Matrices for the 3 DOF Vehicle Model

$$\mathbf{A} = \begin{bmatrix} m_0 & -m_2b & -m_2e & 0 \\ m_1b & I_1 & 0 & -C_\phi \\ -m_2e & m_2be & I_2+m_2e^2 & C_\phi \\ 0 & 0 & 0 & 1 \end{bmatrix} \tag{55}$$

$$\mathbf{B} = \begin{bmatrix} -C_Y/u_1 & -m_0u_1-(aC_{Y1}-bC_{Y2})/u_1 & L_2C_{Y2}/u_1 & C_{Y2} \\ -L_1C_{Y1}/u_1 & -m_1bu_1-L_1C_{Y1}a/u_1 & 0 & K_\phi \\ L_2C_{Y2}/u_1 & m_2eu_1-L_2C_{Y2}b/u_1 & -L_2^2C_{Y2}/u_1 & -L_2C_{Y2}-K_\phi \\ 0 & -1 & 1 & 0 \end{bmatrix} \tag{56}$$

where $m_0 = m_1 + m_2$ and $C_Y = C_{Y1} + C_{Y2}$.

3 System Matrices for the Hybrid Vehicle Model

The non-zero elements of the matrix $\mathbf{A}$ are as follows:
$\mathbf{A}(1,1) = m_1+m_2$, $\mathbf{A}(1,2) = -m_2b$, $\mathbf{A}(1,3) = -m_2e$, $\mathbf{A}(2,1) = m_1b$, $\mathbf{A}(2,2) = I_1$, $\mathbf{A}(3,1) = -m_2e$, $\mathbf{A}(3,2) = m_2be$, $\mathbf{A}(3,3) = I_2+m_2e^2$, $\mathbf{A}(4,4) = 1$, $\mathbf{A}(5,5) = \sigma_yR$, $\mathbf{A}(6,6) = \sigma_yR$, $\mathbf{A}(7,4) = A_pd/Q_{max}$, $\mathbf{A}(7,7) = V_{m0}P_s/(2BQ_{max})$, $\mathbf{A}(8,8) = V_{m0}/Q_{max}$, $\mathbf{A}(9,9) = \sigma_tR$, $\mathbf{A}(10,10) = \sigma_tR$, $\mathbf{A}(11,11) = \sigma_xR$, $\mathbf{A}(12,12) = \sigma_xR$, $\mathbf{A}(13,13) = I_w$, $\mathbf{A}(14,14) = I_w$.

The non-zero elements of the matrix $\mathbf{B}$ are as follows:
$\mathbf{B}(1,2) = -(m_1+m_2)u_1$, $\mathbf{B}(1,5) = 1$, $\mathbf{B}(1,6) = 1$, $\mathbf{B}(2,2) = -m_1bu_1$, $\mathbf{B}(2,5) = L_1$, $\mathbf{B}(2,7) = -A_pdP_s$, $\mathbf{B}(2,9) = 1$, $\mathbf{B}(2,11) = t_a$, $\mathbf{B}(3,2) = m_2eu_1$, $\mathbf{B}(3,6) = -L_2$, $\mathbf{B}(3,7) = A_PdP_s$, $\mathbf{B}(3,10) = 1$, $\mathbf{B}(3,12) = t_a$, $\mathbf{B}(4,2) = -1$, $\mathbf{B}(4,3) = 1$, $\mathbf{B}(5,1) = -C_{y1}$, $\mathbf{B}(5,2) = -aC_{y1}$, $\mathbf{B}(5,5) = u_1$, $\mathbf{B}(6,1) = -C_{y2}$, $\mathbf{B}(6,2) = bC_{y2}$, $\mathbf{B}(6,3) = L_2C_{y2}$, $\mathbf{B}(6,4) = u_1C_{y2}$, $\mathbf{B}(6,6) = -u_1$, $\mathbf{B}(7,4) = -k_0/\phi_{max}$, $\mathbf{B}(7,7) = -(l_0+K_{L0})$, $\mathbf{B}(8,4) = -k_0/\phi_{max}$, $\mathbf{B}(8,7) = -l_0$, $\mathbf{B}(9,1) = C_{t1}$, $\mathbf{B}(9,2) = C_{t1}$, $\mathbf{B}(9,9) = -u_1$, $\mathbf{B}(10,1) = C_{t2}$, $\mathbf{B}(10,2) = -bC_{t2}$, $\mathbf{B}(10,3) = -bC_{t2}$, $\mathbf{B}(10,4) = -u_1C_{t2}$, $\mathbf{B}(10,10) = -u_1$, $\mathbf{B}(11,2) = -2C_{x1}t_a$, $\mathbf{B}(11,11) = -u_1$, $\mathbf{B}(11,13) = -C_{x1}R$, $\mathbf{B}(12,3) = -2C_{x2}t_a$, $\mathbf{B}(12,12) = -u_1$, $\mathbf{B}(12,14) = -C_{x2}R$, $\mathbf{B}(13,11) = R$, $\mathbf{B}(14,12) = R$.

The non-zero elements of the matrix $\mathbf{C}$ are as follows:
$\mathbf{C}(7,1) = k_0/\phi_{max}$, $\mathbf{C}(8,1) = k_0/\phi_{max}$.